Large-Eddy Simulation and experimental study of cycle-to-cycle variations of stable and unstable operating points in a spark ignition engine

V. Granet [a,b,*], O. Vermorel [a], C. Lacour [c], B. Enaux [a,d], V. Dugué [b], T. Poinsot [e]

[a] CERFACS, CFD Team, 42 Av. Gaspard Coriolis, 31057 Toulouse Cedex 01, France
[b] Renault SAS, 1 Av. du Golf, 78288 Guyancourt Cedex, France
[c] IFP Energies Nouvelles, 1 & 4 Av. de Bois-Préau, 92852 Rueil-Malmaison Cedex, France
[d] PSA Peugeot Citroën – DRIA, 2 Route de Gisy, 78943 Velizy-Villacoublay Cedex, France
[e] Institut de Mécanique des Fluides de Toulouse, CNRS, Av. C. Soula, 31400 Toulouse, France

A B S T R A C T

This article presents a comparison between experiments and Large-Eddy Simulation (LES) of a spark ignition engine on two operating points: a stable one characterized by low cycle-to-cycle variations (CCV) and an unstable one with high CCV. In order to match the experimental cycle sample, 75 full cycles (with combustion) are computed by LES. LES results are compared with experiments by means of pressure signals in the intake and exhaust ducts, in-cylinder pressure, chemiluminescence and OH Planar Laser Induced Fluorescence (PLIF). Results show that LES is able to: (1) reproduce the flame behavior in both cases (low and high CCV) in terms of position, shape and timing; (2) distinguish a stable point from an unstable one; (3) predict quantitatively the CCV levels of the two fired operating points. For the unstable case, part of the observed CCV is due to incomplete combustion. The results are then used to analyze the incomplete combustion phenomenon which occurs for some cycles of the unstable point and propose modification of the spark location to control CCV.

Keywords:
Piston engine
Spark ignition
Cycle-to-cycle variation
Large-Eddy Simulation
Chemiluminescence
OH Planar Laser Induced Fluorescence

1. Introduction

The quest for high performances and low emissions leads engineers to trim the operating range of combustion devices near their stability limit. In this context, being able to simulate these devices to predict their stability before building them is of primary importance since experimental campaigns are often very costly. For internal combustion (IC) engines with spark ignition, promising concepts like stratified combustion, lean combustion, direct injection (DI), controlled auto-ignition (CAI) combustion or downsizing have appeared. Downsizing relies on the fact that using an engine at higher loads reduces the fuel consumption. This can be achieved by reducing the engine size. However, for such engines, instabilities like knock, rumble or cycle-to-cycle variations (CCV) need to be controlled. High CCV levels can lead to high pollutants formation, serious drivability issues and, as a consequence, a limited operating range [1].

Most CCV studies have been conducted experimentally [1–7]. Indeed, classical Reynolds-Averaged Navier–Stokes (RANS) simulations, widely used by engineers, only calculate the phase-averaged mean cycle of an engine and cannot reproduce CCV by nature.

The capability of Large-Eddy Simulation (LES) to calculate the unsteady flow field and the increase of computational power have made LES a very attractive tool. Although studies dealing with LES in piston engine for motored engines [8–14] are numerous, few reactive LES of spark ignition engines which aims at reproducing CCV can be found in the literature. The work by Thobois et al. [10] and Richard et al. [15] has shown that LES is intrinsically able to reproduce combustion CCV on mono-cylinder IC engines using classical LES combustion modeling (Thickened Flame model (TFLES) [16] and Coherent Flame Model (CFM-LES) [17,18], respectively). However, the number of simulated cycles was too low (less than 5) in both cases to conclude about the capacity of LES to predict CCV quantitatively and qualitatively. A step forward was achieved in a later study by Vermorel et al. [19] showing good quantitative predictions of CCV on the same engine with a statistical sample of nine cycles. In these studies, for the sake of simplicity and to reduce computational costs, only the engine and a small part of the intake and exhaust ducts were considered in the simulations.

All studies dealing with LES and CCV in the literature had the same drawbacks:

- Too few cycles were computed to get meaningful statistical results. Indeed, a general estimation is that 25 cycles are needed for the mean flow and 50 to ensure a good prediction of cyclic fluctuations [1,20,12].

* Corresponding author at: CERFACS, CFD Team, 42 Av. Gaspard Coriolis, 31057 Toulouse Cedex 01, France.
E-mail address: victor.granet@cerfacs.fr (V. Granet).

- The experimental data available for validating the LES predictions was limited. Typically, only the cylinder pressure curves and their derivative (burnt mass fraction and rate of fuel consumption for instance obtained by 0D combustion analysis) were used to assess the numerical results.

Lacour et al. [21] presented an experimental database of a four-valve single-cylinder spark-ignited piston engine to address these issues. This experimental database was specifically designed for validating LES and many operating points were acquired with or without combustion, with low or high CCV levels. The geometry of the test rig is simple, fully instrumented from the inlet plenum to exhaust. Enaux et al. [22] performed 25 consecutive cycles of the motored operating point where the computational domain included the intake and exhaust plenums and ducts. They presented extended validations in terms of trapped mass, in-cylinder pressure evolution, acoustics in the ducts and velocity fields. Enaux et al. [23] performed 25 consecutive LES cycles of the reference stable (i.e. low CCV) operating point with combustion of the same database. They reported that LES was able to reproduce accurately the range of variability in terms of maximum peak pressure. They also attempted to analyze the sources of CCV and concluded that the velocity field at ignition is crucial in the flame development for this operating point.

Understanding precisely the sources of CCV with LES is not the target of this work. A previous publication by the same authors [23] on the *stab_ref* operating point has shown that large-scale aerodynamic variations, which are well reproduced by LES [22], are the main CCV sources for this engine. In addition, it is well known that many phenomena can lead to CCV [1–5]. All these phenomena are generally linked and interdependent and they also strongly depend on the engine geometry and on the operating conditions as well, which makes difficult to draw general conclusions. This paper aims for a more pragmatic goal: demonstrating that LES can be used to evaluate the stability (in terms of CCV) of a given design and/or operating point. To do so, a stable and an unstable operating point are simulated and compared with detailed experimental results. Among the three unstable operating points (lean combustion, dilution by N_2 and misfiring) available in the experimental database [21,24], the dilution by N_2 was chosen for this work. Indeed, dilution (by N_2 or Exhaust Gas Recirculation (EGR)) is a classical process to reduce *NO* emission [3]. However, with a highly diluted mixture, high CCV may occur and a compromise between reducing *NO* emissions and keeping CCV at an acceptable level must be found.

This paper presents LES of the stable reference and unstable (diluted by N_2) cases, called *stab_ref* and *unst_dil*, respectively, in the remainder of the paper. First, the experimental bench and its characteristics are recalled (Section 2). Second, the numerical setup of the LES is presented (Section 3). Third, the LES results for the *stab_ref* and *unst_dil* operating point are compared with the experimental findings in terms of phase-averaged and variation of in-cylinder pressure and CCV levels (Section 4). LES results are then compared with chemiluminescence and OH Planar Laser Induced Fluorescence (PLIF) diagnostics. Finally, Section 5 presents a discussion on incomplete combustion phenomena occurring for some cycles of the unstable point and how LES can be used to solve this issue.

2. Experimental setup

The SGEmac experiment [21,24] was designed for LES validation: (1) the geometry is simple which eases the definition of the boundary conditions for LES; (2) the experimental operating points are acquired using a premixed gaseous fuel to limit the number of physical models and the modeling difficulties; (3) the operating points acquired experimentally include stable and unstable points to assess the ability of LES to predict CCV levels; (4) the experimental diagnostics are numerous to compare the in-cylinder dynamics, the acoustic behavior in the ducts and the flame propagation with LES. The single-cylinder is a four-valve, pent-roof, spark ignition engine with a flat piston. The whole setup is displayed in Fig. 1a and the main parameters are summarized in Table 1.

The matrix of operating points which includes fired and nonfired points is detailed in [21]. For all fired points, the test bench is fueled with gaseous propane. Air and propane flow rates are controlled by sonic nozzles. Air is introduced in a first plenum and propane is added in a second, mixing plenum. At the engine exhaust, gases flow through a third plenum. Since the engine is operated in a fully premixed mode, a flame-arrestor is added for safety reasons before each plenum (Fig. 1a).

Figure 1b and c show the location of the pressure transducers (which have a one CAD resolution) along the intake (1, 2 and 3) and exhaust ducts (4). Chemiluminescence and OH PLIF measurements are performed through optical windows. The LIF plane is located 8 mm below the spark plug and each image is recorded through the transparent pent-roof. Due to the pent-roof dimension, the whole combustion chamber cannot be visualized. Thus, a small part on both sides of each PLIF image does not contain any experimental data.

Among the various operating points, two were retained for this study: a stable one (*stab_ref*) and an unstable one (*unst_dil*) (Table 2). To ensure proper statistics, 100 for *stab_ref* were measured and 200 cycles for *unst_dil*. The Indicated Mean Effective Pressure (IMEP) remains similar for the two points.

The intake pressure measured in the plenum (Fig. 1b) is around 0.45 for *stab_ref* and 0.6 bar for *unst_dil*. The pressure signals at the exhaust plenum are very similar for both operating points (around 1 atm).

Figure 2 shows the evolution of the phase-averaged mean cylinder pressure for the two fired operating points and also for the motored operating point simulated in [22]. For *stab_ref*, a difference in the pressure signal between the motored and fired conditions is noticeable only around 15 CAD after ignition (which occurs at −20 CA). Afterward, the flame propagates in the combustion chamber and the pressure rise due to combustion reaches around 20 bars for *stab_ref*. The *unst_dil* point, which is fired early (−50 CA) in the compression, presents a peak pressure lower than *stab_ref* despite a higher trapped mass. This is an early indicator of the lower combustion speed experienced by *unst_dil*.

3. Numerical setup

LES simulations are conducted with the parallel AVBP code [25,26] which solves the compressible multi-species Navier–Stokes equations on hybrid grids with cell-vertex and finite-volume formulation. Second-order spatial and temporal accuracy is achieved in the current study by the use of the centered Lax–Wendroff scheme [27].

The numerical setup has been described in detail in a previous work [22] and is only briefly recalled here. It has shown its capability in reproducing accurately the in-cylinder dynamic and its variability. This study [22] was dealing with the validation of the experimental setup on a motored operating point so the emphasis is set on this section on models which were not presented: the ignition model and the combustion model. These models are the same than the ones used in [23]. Only an additional chemical scheme for the diluted operating point has been developed for the present study.

Inlet and outlet boundary conditions in the plenum are handled by the Navier–Stokes Characteristic Boundary Condition (NSCBC)

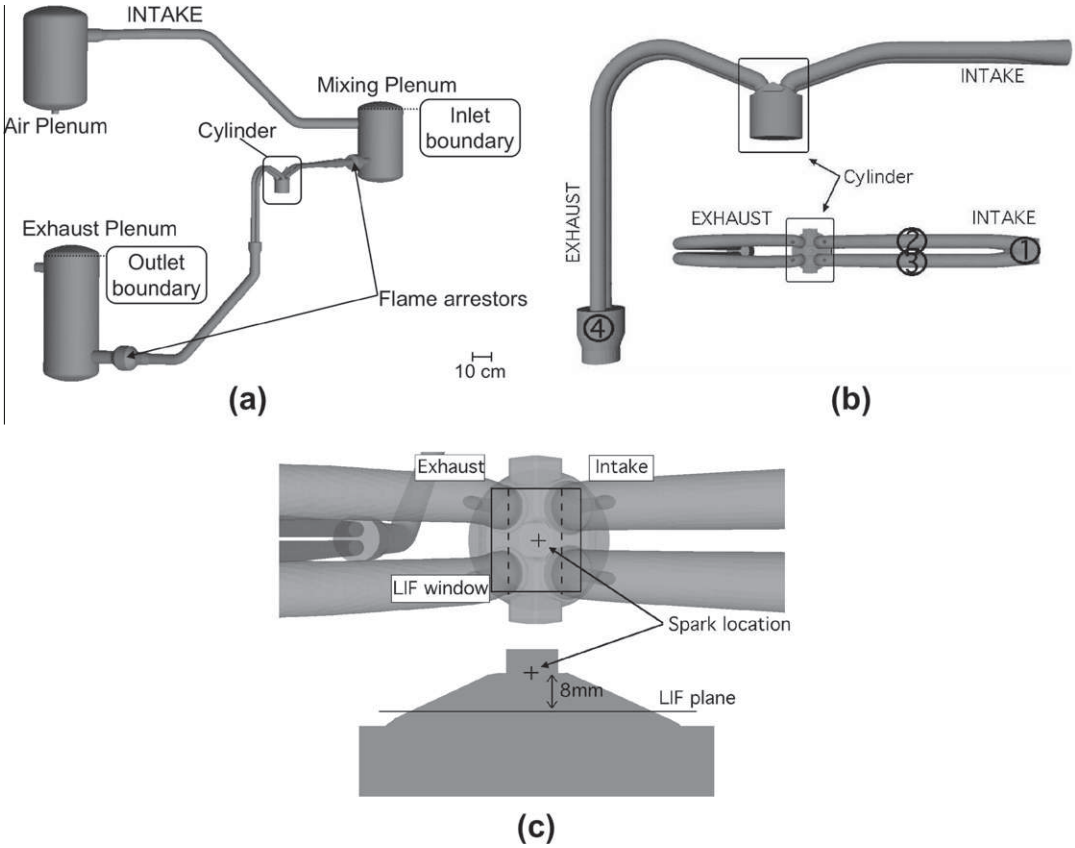

Fig. 1. (a) Experimental bench and locations of the LES boundaries. (b) Location of the experimental measurements: (1, 2, 3, 4) pressure transducers; (c) OH PLIF measurement in an horizontal section of the combustion chamber. The dashed lines in the LIF window represent the limit of the experimental visualization window.

Table 1
Characteristics of the SGEmac engine bench. Crank Angle Degrees (CAD) are relative to compression Top-Dead-Center (TDC).

	Unity	Values
Geometrical compression ratio	(–)	9.9
Engine speed	(rpm)	1200
Bore	(mm)	82
Stroke	(mm)	83.5
Connecting rod length	(mm)	144
Intake Valve Opening (IVO)	(CAD)	350
Intake Valve Closing (IVC)	(CAD)	−120
Exhaust Valve Opening (EVO)	(CAD)	120
Exhaust Valve Closing (EVC)	(CAD)	−350

Table 2
Experimental characteristics of the two simulated fired operating points: *stab_ref* and *unst_dil*.

	Unity	*stab_ref*	*unst_dil*
Fuel	(–)	C_3H_8	
Equivalence ratio	(–)	1	
Number of cycles	(–)	100	200
Dilution by N_2	(% vol.)	0	32
Trapped mass	(mg)	180	250
Ignition timing	(CAD)	−20	−50
Mean IMEP	(bars)	2.97	3.19
COV (IMEP)	(%)	0.76	7.2
Mean P_{max}	(bars)	19.7	16.9
COV (P_{max})	(%)	4.7	12.4

formalism [28,29]. An isothermal law of the wall formulation is used for all walls [30]. The formulation of Cook and Cabot [31] is used to deal with shocks occurring at valves opening. Subgrid

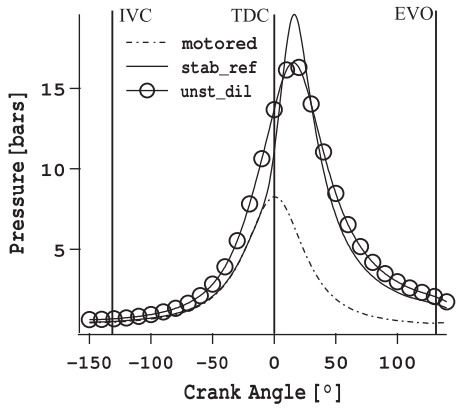

Fig. 2. Evolution of the cylinder pressure of the mean experimental cycle for the two fired operating points. The corresponding motored mean experimental cycle extracted from [22] is superposed for comparison.

stresses are described by the Smagorinsky model [32]. The flame-arrestors play a role on acoustics and their effects are modeled using the model of Mendez and Eldredge [33]. Moving boundaries are handled via an Arbitrary Lagrangian Eulerian (ALE) method combined with a Conditioned Temporal Interpolation (CTI) technique [13]. For each cycle, 43 grids (tetrahedral elements) are used to describe the intake, compression, expansion and exhaust strokes. The grid sizes range from 2.2 millions cells, at TDC, to 9.5 millions at intake and exhaust valve closures. The mesh resolution which is around $\Delta x = 0.8$ mm in the cylinder (which ensures that at least 90% of the kinetic energy is resolved on the LES grid during most part of he cycle) is increased to reach $\Delta x = 0.2$ mm

Table 3
Arrhenius parameters for the C_3H_8 – *BE2* and the C_3H_8 – *VG2* – *DIL* scheme. E_a is the activation energy and *A* the pre-exponential factor.

	C_3H_8 – *BE2* scheme				C_3H_8 – *VG2* – *DIL* scheme			
	C_3H_8 oxidation		$CO–CO_2$ equ.		C_3H_8 oxidation		$CO–CO_2$ equ.	
E_a (cal/mol)	3.4×10^4		1.2×10^4		3.4×10^4		1.2×10^4	
A (cm^3/mol s)	5.8232×10^{12}		2.0×10^9		2.57×10^{12}		2.0×10^9	
Reaction	$n_{C_3H_8}$	0.8	n_{CO}	1.00	$n_{C_3H_8}$	0.8	n_{CO}	1.00
Exponents (–)	$n_{O_2,1}$	0.86	$n_{O_2,2}$	0.50	$n_{O_2,1}$	0.86	$n_{O_2,2}$	0.50

around the position of the spark plug during ignition. The mesh is refined near the spark location to get 10 points within the ignition sphere. This avoids a steep source term which can be difficult to handle numerically. To properly resolve the flow around the valves during valve opening and closing, the mesh is refined around the valves seat with a resolution of $\Delta x = 0.04$ mm.

Flame/turbulence interaction is modeled by the dynamic TFLES model [16] combined with the efficiency function of Colin et al. [16]. The TFLES model is well suited for the perfectly premixed flames encountered in the present study. Furthermore, this combustion model has been successfully used in piston engine [10] as well as gas turbines [34–37] applications. The constant of the efficiency function has been set to 2.0 in the present study. For all the cycles of both operating points, this constant has been kept the same. At the high pressures encountered during the combustion phases, the flame thickness become very small (typically 58 μm at 5.4 bars) for *stab_ref* and the thickening factor can reach values close to 50. For *unst_dil*, flames are slower and thicker and the thickening factors are smaller than 8. Ignition is modeled by the Energy Deposition (ED) model [38,39] which consists in an addition of a source term (gaussian in space and time) in the energy equation. In the experiment, neither the energy transferred to the gas nor the ignition duration is known. The distance between the electrodes in 1.2 mm. To mimic the ignition, the energy duration is set to 100 μs in the simulation. This duration is representative of the glow phase described by Maly and Vogel [40]. The sphere of ignition in the simulation is bigger than the distance between the electrodes in the experiment due to previously mentioned resolution issues. The diameter used in the LES for the ignition sphere is 2.5 mm. The total energy delivered to the gas is 20 mJ, which corresponds to 10% of the overall energy provided by the electrical spark [40,41].

One chemical scheme has been created for each operating point. The two propane/air chemical schemes take into account five species and two reactions (Eqs. (1) and (2) and Table 3):

$$C_3H_8 + 3.5O_2 \rightarrow 3CO + 4H_2O \quad (1)$$

$$CO + 0.5O_2 \rightleftharpoons CO_2 \quad (2)$$

Both schemes were fitted to reproduce adiabatic flame temperature and flame speeds for the corresponding regimes ($C3_{H8}$ _ *BE2* for *stab_ref* and C_3H_8 _ *VG2* – *DIL* for *unst_dil*) during the whole combustion phase.

Figure 3 compares the flame speed variations for an isentropic compression of the fresh gases obtained with the reduced mechanisms to references found in the literature [42,43]. The predicted flame speeds present reasonable agreement with the references. Considering the large error margin on flame speeds at high pressures and temperatures even with detailed mechanisms such as Jerzembeck et al. [43], the precision given by the two-step schemes is sufficient.

4. LES results versus experiments

Based on previous works [44,20,12,19], the number of cycles needed to reproduce the statistics obtained by experiments is typically 25 cycles for mean values and 50 for cycle-to-cycle fluctuations. The work presented in [22] confirmed these values by analyzing experimental data obtained for low CCV conditions. They might not hold for unstable operating points which are more fluctuating by definition. In the present work, 25 consecutive cycles have been performed for *stab_ref* and 50 for *unst_dil*.

The turnover time for a cycle is about 31 CPU h on 400 processors of a SGI Altix ICE 8200 cluster, so that the total computational time reaches 1,200,000 CPU h. For each operating point, the initial solution of the first cycle is the solution obtained after the last cycle computed for the motored case [22]. The resulting initialization cycles (2 for *stab_ref* and *unst_dil*), for which the trapped mass differs from the experimental one, are not considered for statistics.

Table 4 shows the trapped mass and the Internal Gas Recirculation (IGR) for each operating point. The trapped mass is very close

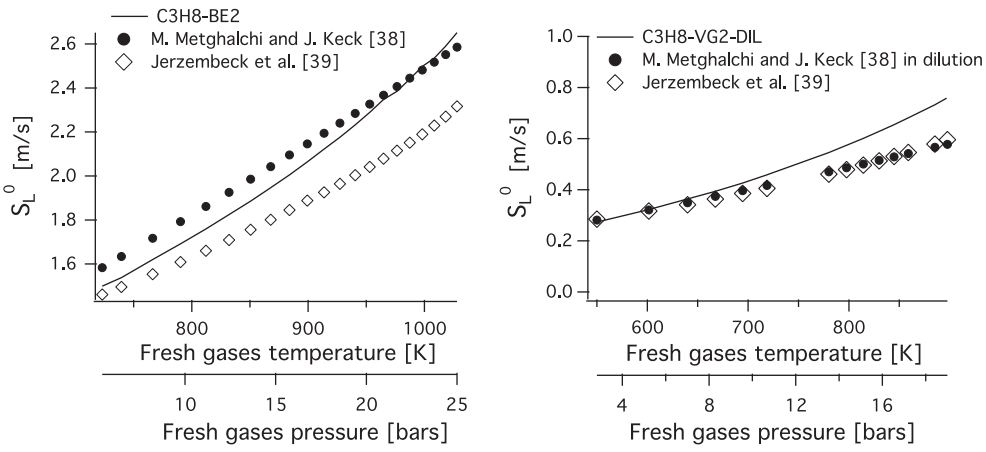

Fig. 3. Comparison between the laminar flame speed found in the literature and the ones predicted by the reduced chemical schemes used in this study: C_3H_8 – *BE2* used for *stab_ref* (left) and C_3H_8 – *VG2* – *DIL* used for *unst_dil* (right).

Table 4
Mean and coefficient of variation of the trapped mass and the IGR for *stab_ref* and *unst_dil*.

		stab_ref		*unst_dil*	
		Mean (mg)	COV (%)	Mean (mg)	COV (%)
Experiments	Trapped mass	180	0.2	250	0.1
LES	Trapped mass	180.3	0.1	251	0.3
	IGR	22.3	2.0	100.0	0.7

to the experiments for both cases. The cyclic variation for both variables is very low. The coefficient of variation (COV), which is the standard deviation divided by the mean (Eq. (3)), achieved experimentally for the trapped mass is 0.2% for *stab_ref* and 0.1% for *unst_dil*.

$$\mathrm{COV}(trapped) = \frac{\sigma_{trapped}}{\overline{trapped}} \times 100 \tag{3}$$

The IGR proportion is large for *unst_dil* since it represents about 40% of the overall mass trapped in the cylinder.

Fig. 4 shows the evolution of the phase-averaged mean pressure at probes 1, 2 and 4 of Fig. 1b. The agreement between the simulation and the experiments is excellent on all probes. This shows that acoustics in intakes and exhaust ducts are correctly captured. It is also consistent with the fact that the volumetric efficiency (filling of the cylinder) is correctly controlled because intake acoustics largely control this quantity. Note that additional tests (not shown here) show that, if the flame-arrestors were not accounted for, the amplitude of these signals would not be damped and would not match experimental results [22].

The comparison between LES and experiments is organized as follows:

- First, the description of the phase-averaged and cycle-by-cycle in-cylinder pressure evolution is presented (Section 4.1).
- Second, the CCV are estimated by the use of the peak pressure, IMEP and chosen CA*X*, where *X* represents a given fraction of burnt fuel and CA*X* the crank angle value at which this fraction is reached (Section 4.2).
- Then, flame kernel growth and propagation extracted from LES are checked against chemiluminescence and OH PLIF measurements (Section 4.3).

4.1. In-cylinder pressure

Fig. 5 presents the evolution of the phase-averaged in-cylinder pressure for the two operating points. The phase-averaged mean cycle is very well reproduced by LES. Combustion is faster for *stab_ref* than for *unst_dil*. For the *stab_ref* case, a slight delay of 2–3 CA is visible on the LES curve compared with the experiment.

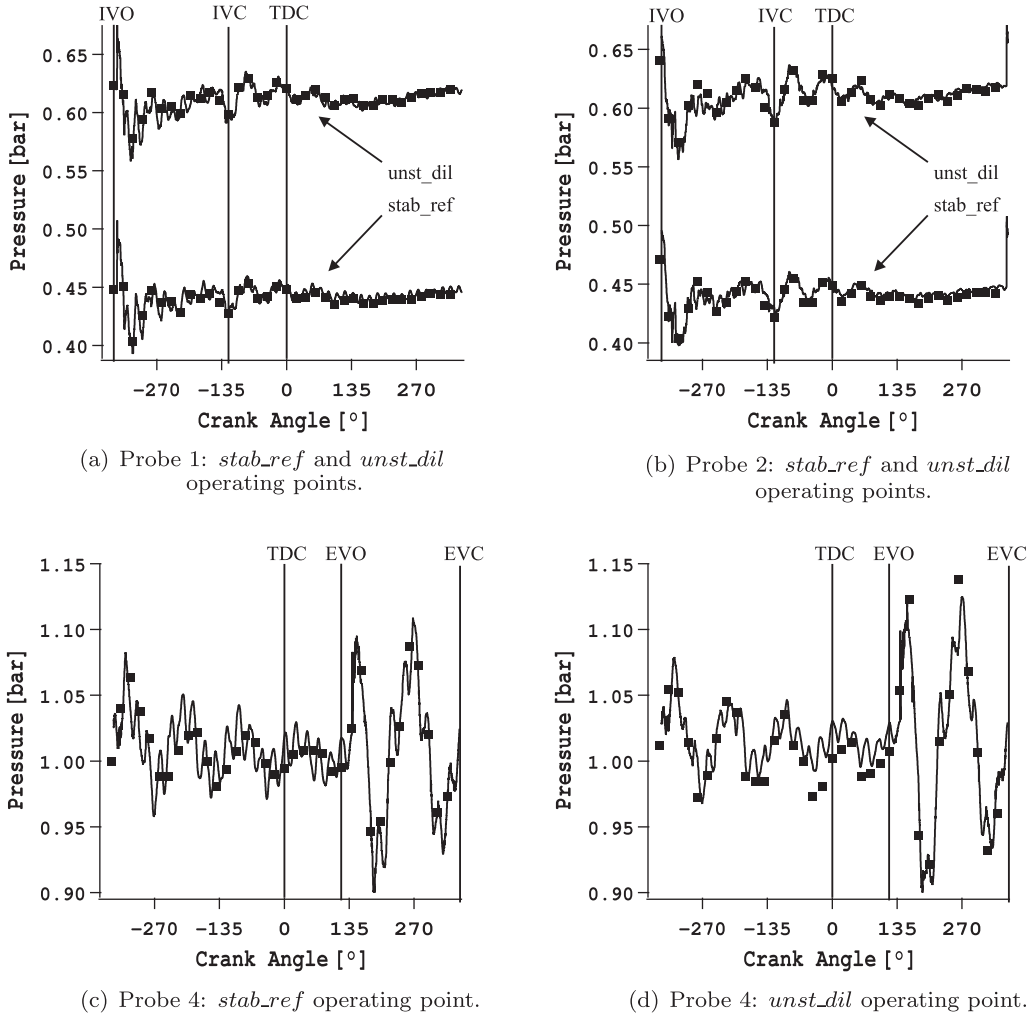

(a) Probe 1: *stab_ref* and *unst_dil* operating points.

(b) Probe 2: *stab_ref* and *unst_dil* operating points.

(c) Probe 4: *stab_ref* operating point.

(d) Probe 4: *unst_dil* operating point.

Fig. 4. Phase-averaged mean pressure at measurements noted 1, 2 (intake ducts) and 4 (exhaust duct), respectively, in Fig. 1b. LES: —; experiments: ■.

Several hypothesis may be ventured to explain this delay: (1) a failure of the 2-step chemical mechanism to reproduce the response of the flame to strain rate, especially in the first times after ignition when the laminar kernel is strongly curved; (2) an insufficient wrinkling of the resolved flame, this issue could be solved by a dynamic calculation of the wrinkling factor or by solving for a transport equation for the wrinkling; (3) an underestimate of the SGS turbulent velocity which leads to a too low value of the efficiency function of the combustion model or (4) an ignition model which is too far from the reality (where the sparking characteristic time is very small), this issue can be solved by using a more complex ignition model such as the ISSIM (Imposed Stretch Spark Ignition Model) model [45] which allows flame distortion by the flow during ignition and estimates the deposited energy from the electrical spark system.

Figure 6 shows the evolution of the cylinder pressure for experiments and LES for each operating point (only the first 100 experimental cycles are shown for *unst_dil* for the sake of clarity). LES reproduces the overall behavior of each operating point. For *stab_ref* (Fig. 6a and b), once the combustion has started, the flame propagation is very fast resulting in steep pressure curves. After peak pressure, the cyclic dispersion goes down quickly and all cycles are almost superimposed during the expansion stroke. This is expected since the trapped mass is almost constant cycle-by-cycle and all the fuel is burnt for each cycle. The phase-averaged mean pressure is around 19 bars and cyclic variations are low. For *unst_dil* (Fig. 6c and d), the pressure curves are more distributed, combustion is slower and occurs later in the cycle. Even though ignition takes place at −50 CA, all cycles remain similar until −10 CA due to a very slow rate of heat release. For both experiments and LES, some cycles hardly reach pressures higher than the motored case presented in Fig. 2. For these cycles, incomplete combustion takes place with a residual fuel mass up to 6% of the trapped one, explaining the variability observed during the expansion stroke.

The Matekunas diagram [4] is another way to characterize cyclic variations using in-cylinder pressure data. The diagram displays the maximum in-cylinder pressure P_{max} versus the crank angle at which it occurs CAP_{max} for all the individual cycles of a given operating point. It provides a direct observation of cyclic combustion variations since mass-burning rate variations produce variations in CAP_{max} as well as change in level of P_{max}. Matekunas identified three zones in this diagram: a "linear" zone where a linear relation exists between P_{max} and CAP_{max}, a "hook-back" zone where P_{max} changes remarkably while CAP_{max} does not and a "return" zone which corresponds to a low level in peak pressure where the slope of mass-burning rate curve is less steep than the volume-rate one.

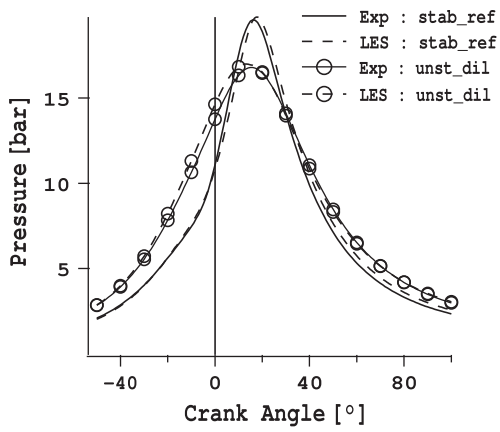

Fig. 5. Evolution of the phase-averaged in-cylinder pressure for the two operating points: comparison between experimental findings and LES.

Figure 7 reproduces this diagram for the two operating points. The *stab_ref* operating point stands right in the "linear" zone of the Matekunas diagram which also corresponds to fast combustion. This indicates a low level of CCV for the *stab_ref* point for both experiments and LES. The *unst_dil* point however, experiences cycles in all three zones for both experiments and LES: the burning rates and phasing of each cycle are very different from one cycle to another due to the high CCV.

4.2. Estimation of CCV

The most commonly used variables as CCV indicators are the coefficient of variation in maximum pressure and in IMEP [1,3,46]. The IMEP represents the averaged pressure of a given cycle. Heywood [1] reported serious drivability issues for COV (IMEP) higher than 10%. Dec [46] estimated an acceptable limit, at which the engine switches from stable to unstable, at 2% for PRF80 (a mixture consisting of 80% iso-octane and 20% *n*-heptane).

This section addresses two questions: (1) is LES able to distinguish between a stable and an unstable operating point with a reasonable number of cycles? (2) is LES able to predict values of the CCV for each operating point while simulating 25 cycles for *stab_ref* and 50 for *unst_dil*?

Figure 8 presents the COV (P_{max}) against the COV (IMEP) for the experiments and LES, taking into account only 25 cycles in one set of statistics. Experimentally, for *stab_ref* the COV (IMEP) varies from 0.5% to 0.9% and 4.6% to 9.1% for *unst_dil*. This means that 25 cycles are enough to identify stable or unstable cases. LES provides the same conclusions: it leads to 0.5% of COV (IMEP) for the single *stab_ref* set and to 6.1% and 9.6% for the two data sets of *unst_dil* for which 50 cycles are available. These results are coherent with the previously mentioned literature [1,46].

As seen in Figure 8, 25 cycles are not enough to get converged statistics for *unst_dil*, since the values of COV (IMEP) and COV (P_{max}) are noticeably different for experimental (and LES) sets. To determine how many cycles would be needed to get converged statistics, the evolution of COV (P_{max}) and COV (IMEP) is plotted in Fig. 9 as a function of the number of cycles used for statistics. For the experiments, both indicators can be used to determine whether the point is stable or not as soon as more than 10 cycles are available. Moreover, both indicators indicate that after 25 cycles the *stab_ref* point is near its final value of CCV. For *unst_dil*, around 70 cycles are needed to ensure proper convergence. LES seems to reproduce the same rate of convergence than the experiments for both operating points even if more cycles would be clearly needed to conclude.

Figure 10 displays the cycle-by-cycle evolution in terms of combustion duration for the two operating points: the CA2, CA50 and CA90 extracted from the Burnt Mass Fraction (BMF) evolution calculated with a 0D adiabatic combustion analysis tool [1] are presented for all the experimental and LES cycles. This combustion analysis tool, assuming a constant heat capacity ratio, calculates the BMF with the use of the in-cylinder pressure, species mass fraction and volume. The same tool is used to process the experimental and LES data to ensure a fair comparison. Differences between CA*X* are used to calculate the duration of each characteristic phase of combustion [1,3]:

- CA2-CAIGN: duration of combustion to burn a small but significant fraction of the cylinder mass.
- CA90-CA2: duration during which most of the charge is burnt.
- CA90-CAIGN: duration of the overall combustion process.

The CA50 is representative of the phasing of a cycle. Combustion duration is around 100 CAD for *unst_dil*, whereas only 40°

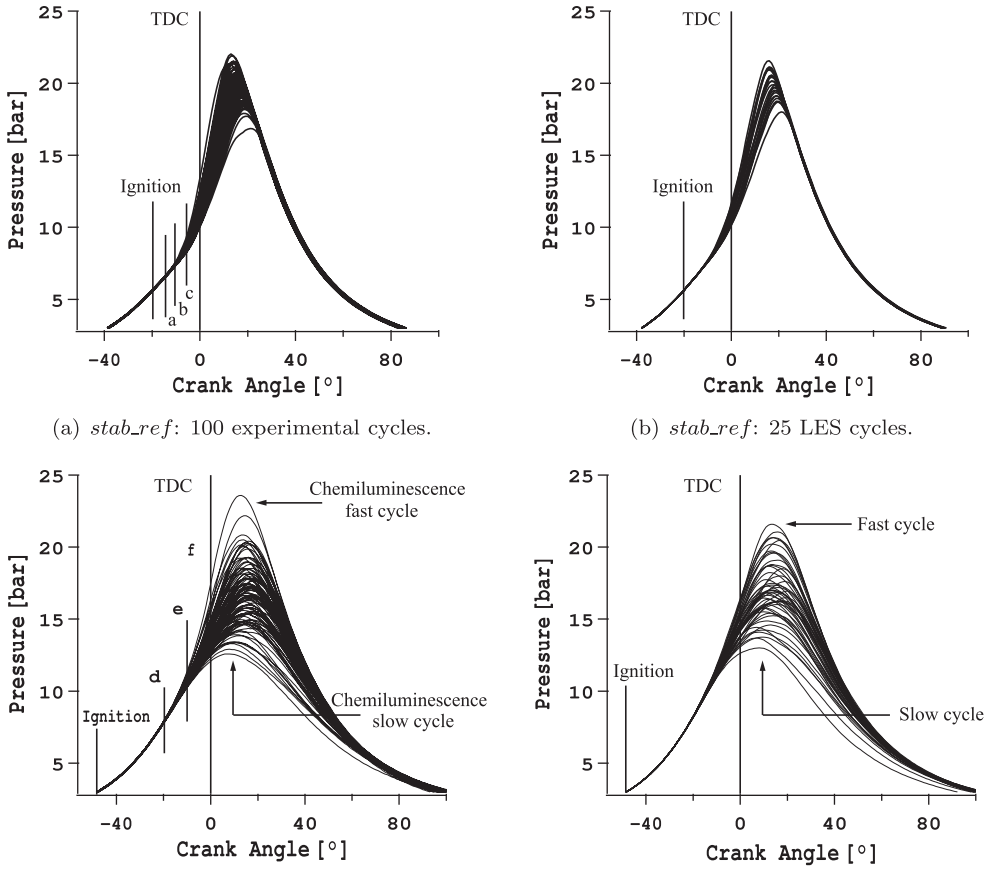

(a) *stab_ref*: 100 experimental cycles. (b) *stab_ref*: 25 LES cycles.

(c) *unst_dil*: 100 experimental cycles. (d) *unst_dil*: 50 LES cycles.

Fig. 6. Evolution of the cylinder pressure for each operating point: comparison between experimental findings (left) and LES (right). The noted letters a to f show the crank angles at which the chemiluminescence images shown in Section 4.3 are acquired.

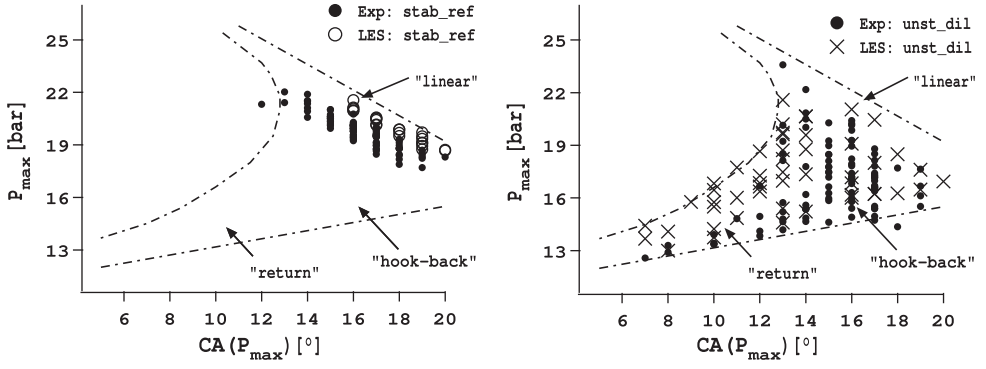

(a) *stab_ref* (b) *unst_dil*

Fig. 7. Maximum pressure against CAP_{max} for *stab_ref* (left) and *unst_dil* (right). The first 100 experimental cycles of the 200 cycles acquired for *unst_dil* are plotted for sake of clarity.

are needed for *stab_ref* to burn the in-cylinder fuel. These 40° actually correspond to the CA2 for *unst_dil* where only a very limited part of the charge has burned. LES predicts very well the CA2 but slightly overestimates the CA50 and CA90 mean values. This longer combustion process may seem inconsistent with the higher P_{max} observed in Fig. 7 in the LES. A couple of explanations can be drawn to explain this issue: (1) fuel storage in crevices during the compression stroke and release in the cylinder during the expansion stroke and (2) compression of the elongated piston. This feature was already noted (the actual compression ratio in the experiments was different than the geometric one) in a previous publication [22] while simulating the motored operating point. After CA50, the flame interacts strongly with the walls making the estimation of heat transfer of primary importance. However, the calculation of the heat fluxes in the LES is most likely to be delicate since no precise temperature values are available from the experiments. Setting up a specific strategy like coupling with a code dedicated to heat transfer could solve this issue.

The magnitude of the coefficient of variation of each CA is also well reproduced by LES: for *stab_ref* the coefficient of variation of CA2 is around 5% and decreases at CA50 and CA90. For *unst_dil* the CA2 value is also around 5% but the coefficient of variation of

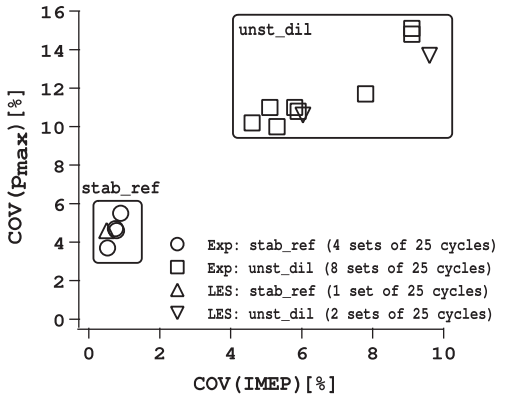

Fig. 8. Comparison of variation of the coefficient of variation of the maximum pressure and IMEP for experimental and LES sets of 25 cycles.

each remaining CA is much higher: the variability is enhanced by the very long combustion process. This suggests that the early propagation is a key stage for *stab_ref* (which is coherent with the findings reported in [23]) and for *unst_dil*.

To verify this observation, Fig. 11 shows that the correlation between the CA2 and CA90 is very similar for the two operating points. For both experiments and LES the early propagation is the key element to explain the burning rate of a given cycle. It means that the increase in the coefficient of variation of the CA*X* for *unst_dil* is only due to the duration of the combustion process: since the combustion is slow, each cycle has more time to drift away from other cycles.

4.3. Analysis of flame shapes

The flame position is characterized experimentally using chemiluminescence and OH PLIF. Chemiluminescence is a line of sight technique which allows a flame visualization integrated in the chamber throughout the whole combustion process. OH PLIF is used to visualize a 2D slice of the flame location, timing and shape in a plane 8 mm below the spark plug.

Figures 12 and 13 display the flame propagation in the experiments and in the LES of a chosen cycle for *stab_ref* (the experimental and LES cycle present the same peak pressure around 18 bars) and two cycles for *unst_dil* (a fast cycle and a slow cycle identified in Fig. 6). Of course, comparing individual cycles is difficult and Figs. 12 and 13 are used only to show that, qualitatively, LES and experiments produce the same type of flames. The exact shapes of the front cannot be compared. For *stab_ref* (Fig. 12), the flame is fast and is first convected toward the exhaust valves (located on the left of the pictures) by the tumble motion in the cylinder. It consumes the rest of the fuel on the left side before moving toward the right side of the chamber. LES captures this movement with a slight delay as already noticed in Fig. 5. For *unst_dil* (Fig. 13), the flow affects more the flame growth: the initial kernel is convected far away from the spark plug for the fast cycle and the flame is more wrinkled by turbulence. For the slow cycle, the flame fails to propagate early in the cylinder in both experiments and LES. At −20 CA, the slow cycle exhibits a flame front which is cut in two by its interaction with the wall. The smaller pockets quench, explaining the slow flame growth. This phenomenon is discussed in Section 5.

Figures 14 and 15 show the flame presence probability obtained by the OH PLIF diagnostic. Each experimental PLIF image is binarized (0 in the fresh gases and 1 in the burnt gases) and averaged over 25 cycles. The same procedure is applied to LES temperature fields, where a threshold value of 1500 K is used to binarize the flame presence. The thresholds used for experiments and LES are not the same but additional tests have been conducted with different thresholds and these values do not have a strong effect on the results.

For *stab_ref* (Fig. 14), the expansion of the flame is quite regular in time. The probability is much wider 20° after ignition than 10°

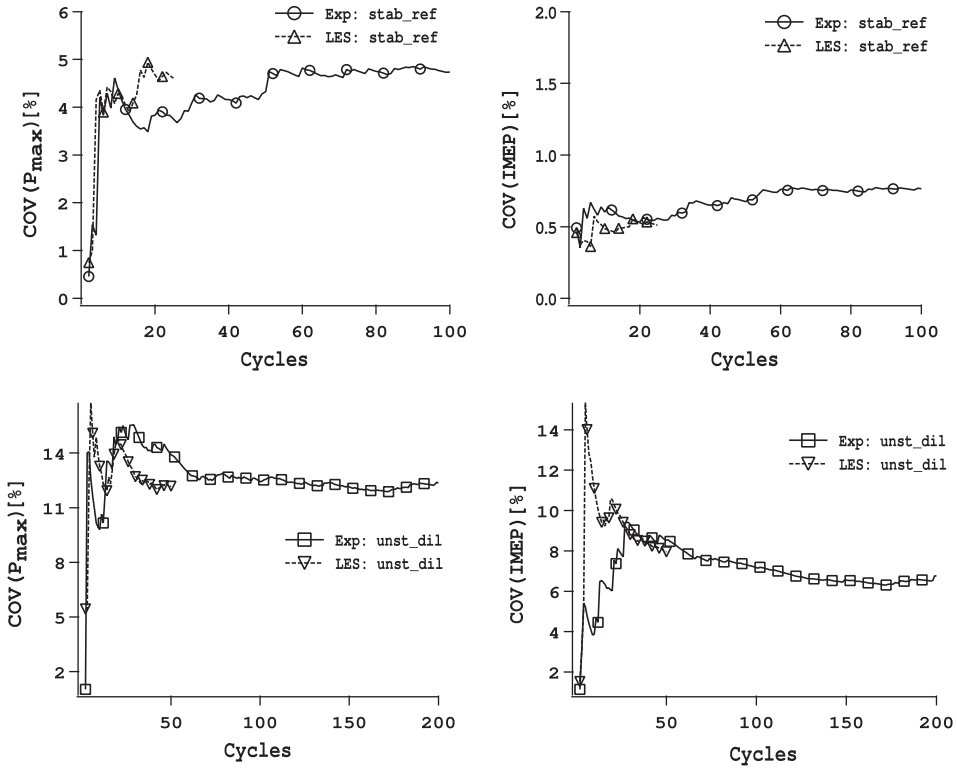

Fig. 9. Comparison of the convergence of the coefficient of variation of the maximum pressure and IMEP for *stab_ref* (top) and *unst_dil* (bottom) between experiments and LES.

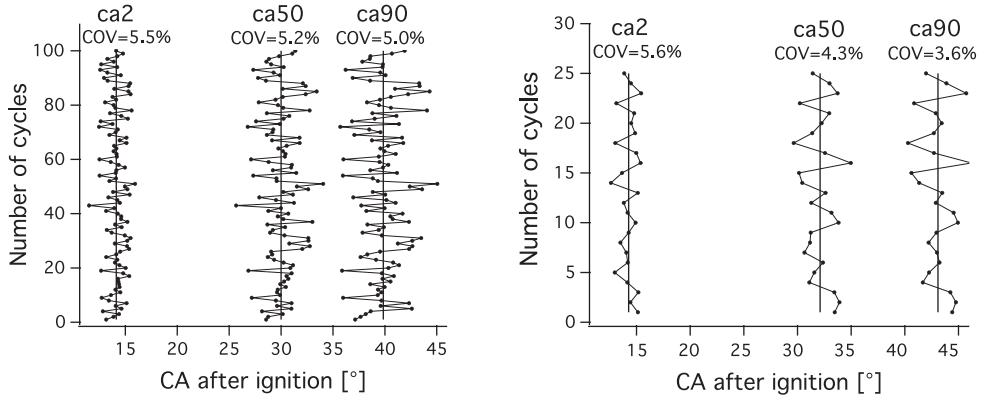

(a) *stab_ref*: 100 experimental cycles (b) *stab_ref*: 25 LES cycles

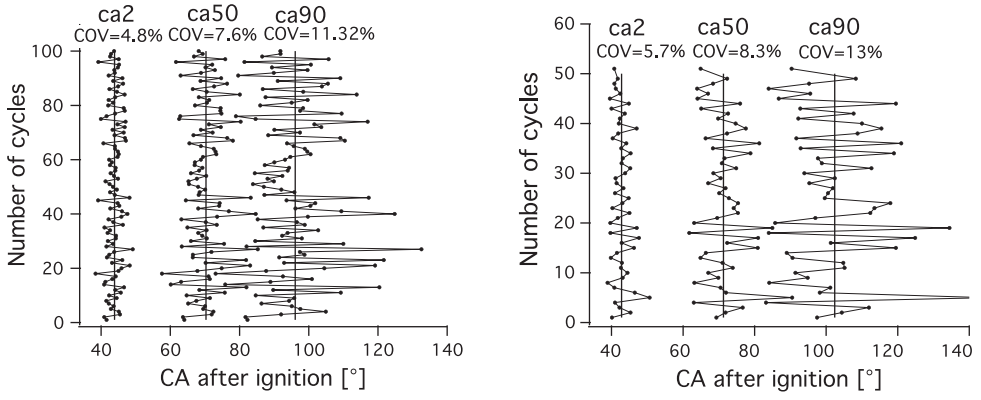

(c) *unst_dil*: 100 experimental cycles (d) *unst_dil*: 50 LES cycles

Fig. 10. Cycle-by-cycle values of the CA2, CA50 and CA90 for the two operating points: -•- individual cycles and – mean value.

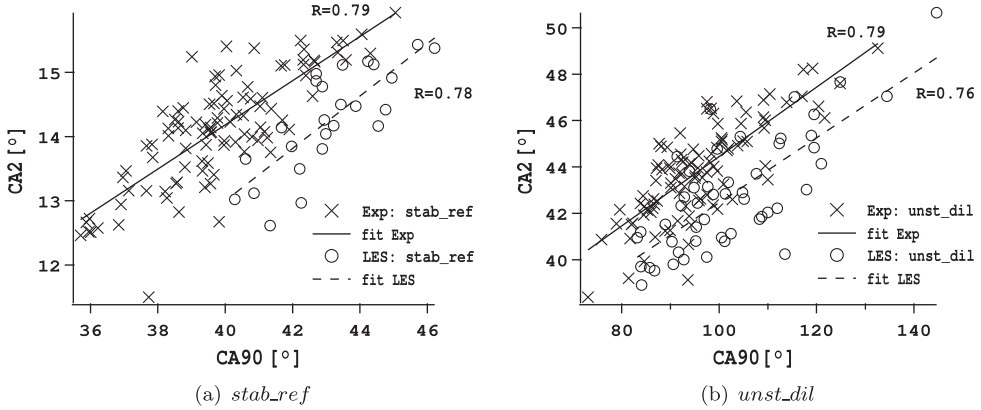

(a) *stab_ref* (b) *unst_dil*

Fig. 11. Correlation between the CA2 and CA90 for experiments and LES for the two operating points. R denotes the Pearson correlation coefficient assuming a linear dependance.

after ignition but still localized on the left side of the combustion chamber. LES reproduces the experimental behavior in terms of shape, position and timing although LES experiences a slight delay previously noticed.

For *unst_dil* (Fig. 15), the flame presence is less intense than for *stab_ref* indicating more dispersion in flame position and shape. LES and experimental maps are similar even if the kernel seems to convect faster toward the exhaust valve in the LES than in the experiments. A possible explanation is that the electrodes of the spark plug can protect the initial kernel from the mean convective flow and anchor the flame in the early times after ignition in the experiments. This effect cannot be reproduced in the computations since the electrodes are not represented in the LES geometry. In addition, due to the position of the pent-roof, it is not possible to visualize experimentally the flame in that region of the cylinder.

5. Discussion

The unstable operating point leads to some cycles where the flame does not manage to burn all the fuel in the cylinder (6% of unburnt fuel); this behavior is unwanted for the design of such an engine since it can cause a severe increase of the pollutant emissions.

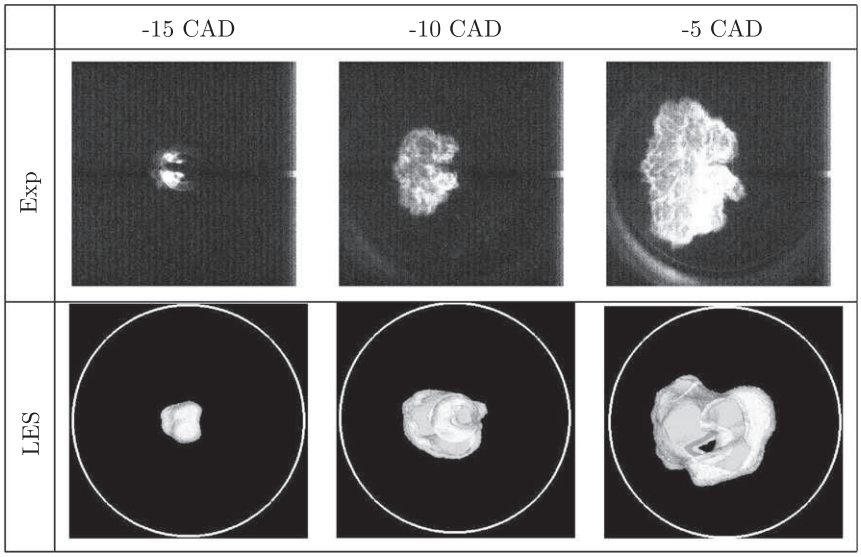

Fig. 12. Chemiluminescence of the flame development of one experimental (top) and LES (bottom, isosurface of heat release) cycle of *stab_ref* at −15 CAD, −10 CAD and −5 CAD (letters a, b and c of Fig. 6a, respectively). Intake (exhaust) valves are located on the right (left) of each picture, respectively.

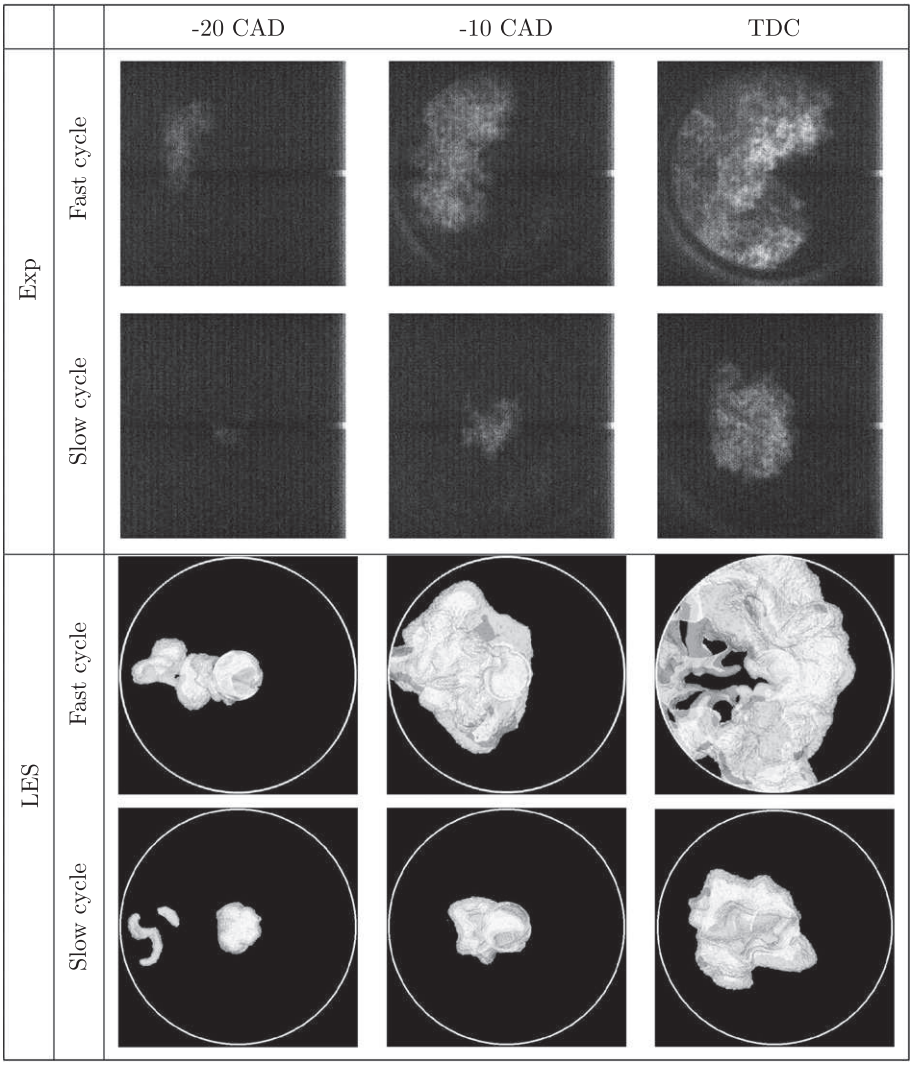

Fig. 13. Chemiluminescence of the flame development of two experimental (top) and LES (bottom, isosurface of heat release) cycles of *unst_dil* at −20 CAD, −10 CAD and TDC (letters d, e and f of Fig. 6c, respectively). Intake (exhaust) valves are located on the right (left) of each picture, respectively.

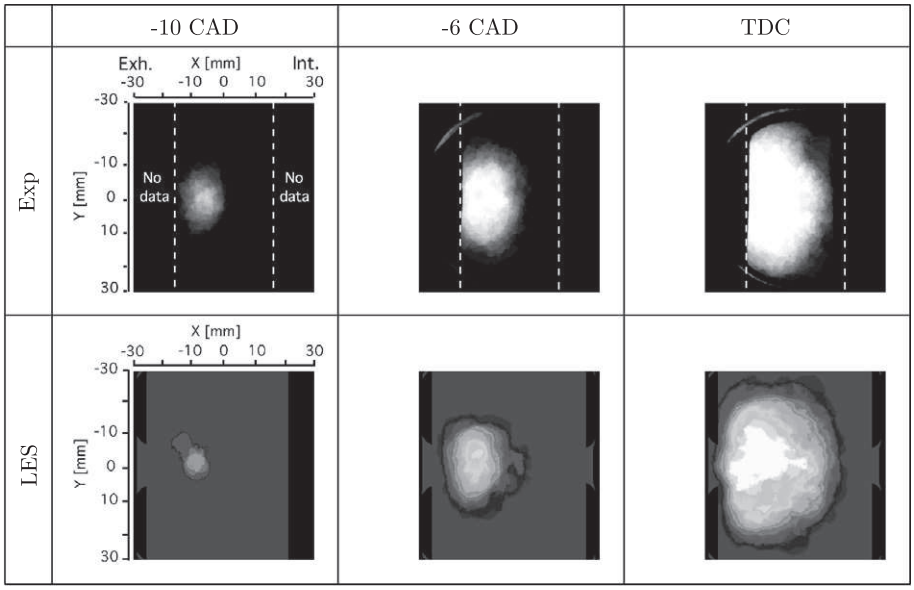

Fig. 14. Flame presence probability extracted from PLIF images for 25 experimental (top) cycles for *stab_ref* at −10 CAD, −6 CAD and TDC (left to right). The white dashed lines represent the limit of the experimental window. Flame presence probability extracted from LES (bottom) are shown as well for 25 cycles. Spark ignition occurs at ($x = 0$, $y = 0$) at −20 CAD.

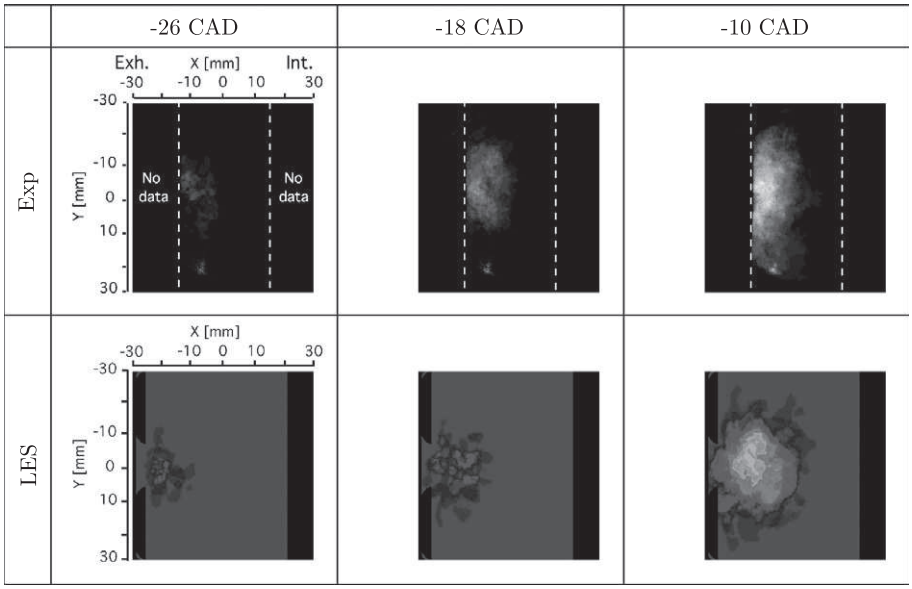

Fig. 15. Flame presence probability extracted from PLIF images for 25 cycles for *unst_dil* at −26 CAD, −18 CAD and −10 CAD (left to right). The white dashed lines represent the limit of the experimental window. Flame presence probability extracted from LES (bottom) are shown as well for 25 cycles. Spark ignition occurs at ($x = 0$, $y = 0$) at −50 CAD.

The focus is put in this section on how LES can be used to: (1) analyze the events which lead to incomplete combustion in *unst_dil* and (2) suggest a solution to avoid incomplete combustion cycles.

To do so, two LES cycles have been chosen: cycle 21 presents a peak pressure near the phase-averaged pressure of *unst_dil* (16 bars); cycle 22 has a very low peak pressure (13 bars) and incomplete combustion occurs. Figure 16 shows a visualization of the flame of cycle 21 and 22 of *unst_dil* at five crank angles. For cycle 21, 8 CA after ignition, the initial kernel splits into two flames at the edge between the spark plug and the cylinder head:

- The first pocket is confined in the spark plug where it can encounter a low turbulence level [23] which guarantees a slow but safe propagation of the flame.
- The second pocket is carried in the cylinder by the flow where the turbulence is much more intense.

This second pocket is not constrained near the wall and can then propagate into the highly turbulent in-cylinder flow (−30 CAD). After its propagation and growth in the cylinder, it merges with the first pocket which had enough time to burn all the fuel in the spark plug region (−20 CAD). Later this flame consumes the fuel remaining on both sides of the cylinder (at TDC).

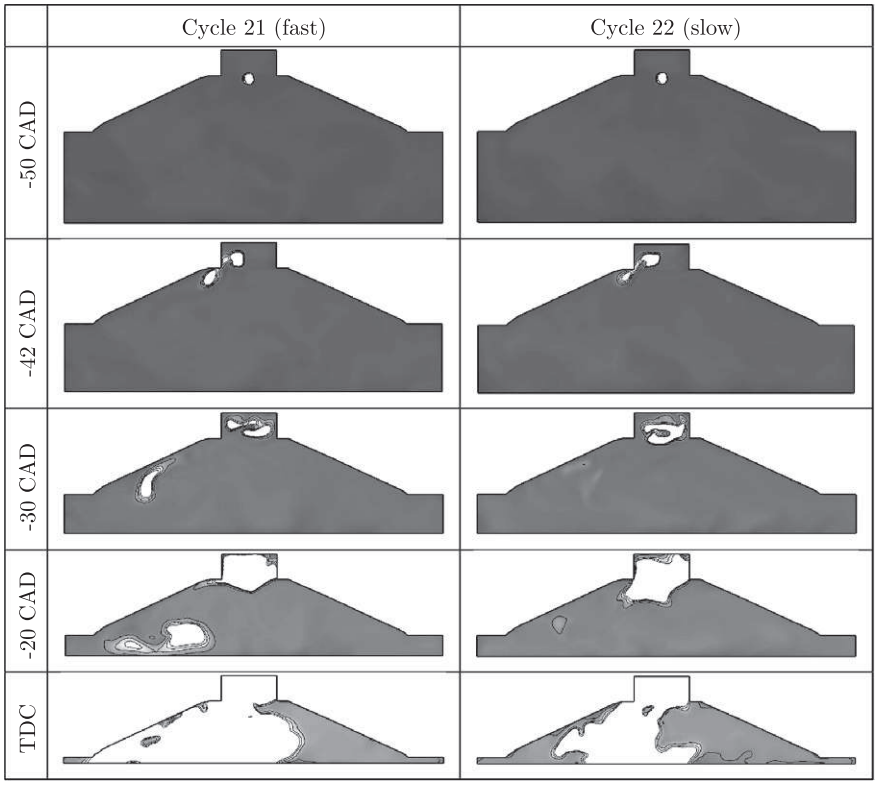

Fig. 16. Temperature field (white: $T > 1400$ K and black: $T = 300$ K) of cycle 21 (left) and 22 (right) for *unst_dil* at five crank angles.

For cycle 22, the second pocket which propagates into the chamber is really small (−42 CAD) and quenches a few CA after the splitting because it is too small and too close to walls. This quenching leads to a very low in-cylinder pressure.

For the *stab_ref* point, the flame does not split and no quenching phenomena take place. Note that, the reported propagation mechanisms for the two operating points for this specific engine cannot be considered as a general criteria that distinguish stable and unstable flame behavior in piston engines. To understand the differences between the two operating points, a dimensionless number is mainly used in the literature: the Damköhler number, Da. It compares the chemical τ_c and flow τ_f characteristic time scales (Eq. (4)).

$$\mathrm{Da} = \frac{\tau_f}{\tau_c} = \left(\frac{l_t}{u'}\right)\left(\frac{s_L^0}{\delta_L^0}\right) \tag{4}$$

where l_t is the integral length scale which is taken as $h_c/6$ [47] with h_c the clearance height and u' the large-scale velocity fluctuations estimated by the formula of Colin et al. [16] which does not take into account the dilatational part of the velocity. Here, δ_L^0 is estimated by the Blint correlation [48] and s_L^0 is recovered from the chemical scheme. These four variables of interest are calculated at ignition and TDC for both operating point in Table 5. The values of the Damköhler and turbulent Reynolds ($\mathrm{Re}_T = \frac{u' \times l_t}{\nu}$) numbers are also given for information. Even though the fields of u' for both operating points are similar, leading to comparable turbulence levels, the laminar flame speed (thickness) is much larger (smaller) for *stab_ref* than *unst_dil*.

The chemical time scale for *unst_dil* is larger than for *stab_ref*, while the flow time scale remains similar: the *unst_dil* flame is going to be more sensitive to turbulence than the *stab_ref* one.

Once the cycles which present incomplete combustion have been isolated, additional LES computations can suggest possible solutions to solve this issue. For the considered engine and operating point, an easy and acceptable solution to burn all the fuel trapped in the cylinder is to ignite 1*mm* lower in the chamber (by using a longer spark for example).

Figure 17 shows the flame of the improved version of cycle 22. The LES computation restarts 1 CA before igniting cycle 22 and the local conditions remain identical. Moving the spark 1 mm lower in the chamber has a direct effect on the flame propagation: a larger part of the flame splits at the edge of the spark plug and cylinder head (−42 CAD). It propagates very fast in the chamber and is not quenched. Thus, the maximum in-cylinder pressure reaches 20.4 bar and all the fuel in the cylinder is burnt.

6. Conclusion

This article presents a detailed comparison between Large-Eddy Simulations (LES) and experiments of a stable (low cycle-to-cycle variations (CCV)) and an unstable (high CCV) fired operating point of a spark ignition engine. The experimental test rig setup of the four-valve single-cylinder is tailored for LES validation. The LES methodology used for this study ranges from the exhaust to the intake plenum to take into account naturally the acoustic in the ducts and simplify the treatment of the boundary conditions. The comparison includes pressure signals in the intake and exhaust

Table 5
Variables of interest at ignition and TDC for both operating points.

	Unity	Ignition		TDC	
		stab_ref	*unst_dil*	*stab_ref*	*unst_dil*
l_t	(mm)	1.95	4.5	1.42	
δ_L^0	(μm)	56	590	37	105
u'	(m/s)	1	1	1.55	1.44
s_L^0	(m/s)	1.58	0.2	1.96	0.49
Da	(–)	310	3	400	30
Re_T	(-)	57	160	59	55

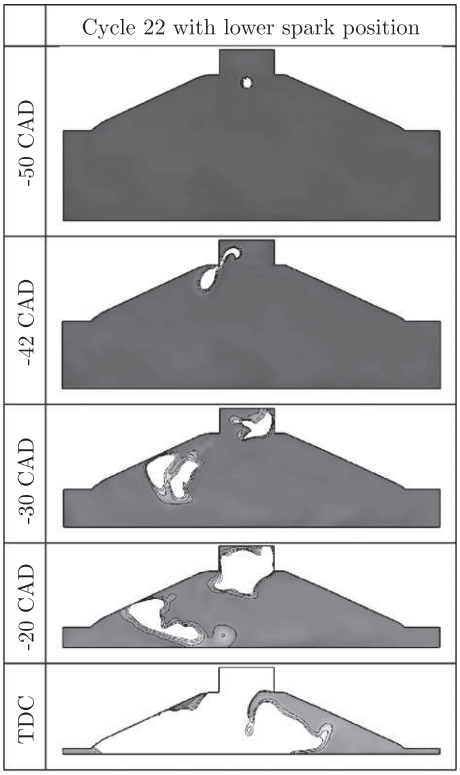

Fig. 17. Temperature field (white: $T > 1400$ K and black: $T = 300$ K) of cycle 22 with a lower spark position for *unst_dil* at five crank angles.

ducts, in-cylinder pressure, chemiluminescence and OH Planar Laser Induced Fluorescence (PLIF).

25 LES cycles of the stable and 50 cycles of the unstable operating point are presented in this study. The detailed comparison between LES results and experiments indicates that:

- LES is able to predict qualitatively and quantitatively the CCV of real fired operating points
- LES is able to distinguish a stable point from an unstable one.
- LES mimics well the evolution of the flame in terms of shape, position and timing (even if a slight delay is observed on most cycles of the stable point).

LES has also been used to analyze and suggest a solution for incomplete combustion which occurs for some cycles of the unstable point. For all cycles, the initial kernel splits into two flame pockets at the corner of the spark plug and cylinder head around 10 crank angle degrees after ignition. For cycles with incomplete combustion, this pocket which propagates in the cylinder quenches later in the cycle. In that case, only the slow burning part of the flame, which is in the spark plug cavity, remains to ensure the flame propagation, leading to incomplete combustion. LES also shows that this can be avoided by using a different spark location: the same cycle was computed again with a spark plug lowered 1 mm in the chamber and lead to complete combustion. Even though this exercise remains purely academical, it shows how LES could be used in the near future to reduce CCV in engines.

These promising results and the observed capacity of the presented LES methodology to reproduce the experimental findings rely strongly here on the correct prediction of aerodynamic variations [22], which were found to be the main sources of CCV [23]. However, this might not be sufficient for other engines where mixture (in the case of Direct Injection configurations especially [12]) or temperature fluctuations might play a key role in the generation of CCV. In particular, the current LES setup probably would not be satisfactory in reproducing temperature variations since the wall's temperatures are considered homogeneous and constant during the whole computation. An extension of the present methodology is currently underway to improve that point coupling a heat conduction solver to the LES solver.

Acknowledgments

The authors gratefully acknowledge the financial support provided by Renault SAS and PSA Peugeot Citroën in the framework of thesis researches. This work was granted access to the HPC resources of CINES under the allocation 2009-c2009026055 made by GENCI (Grand Equipement National de Calcul Intensif). The authors acknowledge the financial support by ANR under Grant no. ANR-06-PDIT-007-01 SGEmac.

References

[1] J.B. Heywood, Internal Combustion Engine Fundamentals, McGraw and Hill Series in Mechanical Engineering, McGraw-Hill, New-York, 1988.
[2] P.G. Hill, Cyclic variations and turbulence structure in spark-ignition engines, Combust. Flame 72 (1988) 73–89.
[3] N. Ozdor, M. Dulger, E. Sher, Cyclic variability in spark ignition engines. A literature survey, SAE paper (950683).
[4] F.A. Matekunas, Modes and measures of cyclic combustion variability, SAE paper (830337).
[5] M.B. Young, Cyclic dispersion in the homogeneous charge spark-ignition engine. A literature survey, SAE paper (810020).
[6] K. Hamai, H. Kawajiri, T. Ishizuka, M. Nakai, Combustion fluctuation mechanism involving cycle-to-cycle spark ignition variation due to gas flow motion in S.I. engines, in: 21st Symposium (International) on Combustion, The Combustion Institute, Pittsburgh, 1986, pp. 505–512.
[7] P.G. Aleiferis, Y. Hardalupas, A.M.K.P. Taylor, K. Ishii, Y. Urata, Flame chemiluminescence studies of cyclic combustion variations and air-to-fuel ratio of the reacting mixture in a lean-burn stratified-charge spark-ignition engine, Combust. Flame 136 (1–2) (2004) 72–90.
[8] D. Haworth, Large-Eddy simulation of in-cylinder flows, Oil & Gas Sci. Tech. 54 (2) (1999) 175–185.
[9] I. Celik, I. Yavuz, A. Smirnov, Large eddy simulations of in-cylinder turbulence for internal combustion engines: a review, Int. J. Eng. Res. 2 (2) (2001) 119–148.
[10] L. Thobois, R. Lauvergne, T. Poinsot, Using LES to investigate reacting flow physics in engine design process, SAE paper (2007-01-0166).
[11] M.S. Toledo, L.L. Penven, M. Buffat, A. Cadiou, J. Padilla, Large eddy simulation of the generation and breakdown of a tumbling flow, Int. J. Heat Fluid Flow 28 (2007) 113–126.
[12] D. Goryntsev, A. Sadiki, M. Klein, J. Janicka, Large eddy simulation based analysis of the effects of cycle-to-cycle variations on air–fuel mixing in realistic DISI IC engines, Proc. Combust. Inst. 32 (2009) 2759–2766.
[13] R. Verzicco, J. Mohd-Yusof, P. Orlandi, D. Haworth, Large eddy simulation in complex geometric configurations using boundary body forces, AIAA J. 38 (3) (2000) 427–433.
[14] V. Dugue, N. Gauchet, D. Veynante, Applicability of Large Eddy Simulation to the fluid mechanics in a real engine configuration by means of an industrial code, SAE paper (2006-01-1194).
[15] S. Richard, O. Colin, O. Vermorel, A. Benkenida, C. Angelberger, D. Veynante, Towards large eddy simulation of combustion in spark ignition engines, Proc. Combust. Inst. 31 (2007) 3059–3066.
[16] O. Colin, F. Ducros, D. Veynante, T. Poinsot, A thickened flame model for large eddy simulations of turbulent premixed combustion, Phys. Fluids 12 (7) (2000) 1843–1863.
[17] S.M. Candel, T. Poinsot, Flame stretch and the balance equation for the flame surface area, Combust. Sci. Tech. 70 (1990) 1–15.
[18] O. Colin, A. Benkenida, C. Angelberger, 3D modeling of mixing, ignition and combustion phenomena in highly stratified gasoline engine, Oil Gas Sci. Tech. 58 (1) (2003) 47–62.
[19] O. Vermorel, S. Richard, O. Colin, C. Angelberger, A. Benkenida, D. Veynante, Towards the understanding of cyclic variability in a spark ignited engine using multi-cycle LES, Combust. Flame 156 (2009) 1525–1541.
[20] I. Celik, M. Klein, M. Freitag, J. Janicka, Assessment measures for URANS/DES/LES: an overview with applications, J. Turb. 7 (48) (2006) 1–27.
[21] C. Lacour, C. Pera, B. Enaux, O. Vermorel, C. Angelberger, T. Poinsot, Exploring cyclic variability in a spark-ignition engine using experimental techniques, system simulation and Large-Eddy Simulation, in: Proceedings of the 4th European Combustion Meeting, Vienna, Austria, 2009.
[22] B. Enaux, V. Granet, O. Vermorel, C. Lacour, L. Thobois, V. Dugue, T. Poinsot, Large Eddy Simulation of a motored single-cylinder piston engine: numerical strategies and validation, Flow Turbul. Combust. 86 (2) (2011) 153–177.

[23] B. Enaux, V. Granet, O. Vermorel, C. Lacour, C. Pera, C. Angelberger, T. Poinsot, LES study of cycle-to-cycle variations in a spark ignition engine, Proc. Combust. Inst. 33 (2) (2011) 3115–3122.
[24] C. Lacour, C. Pera, An experimental database dedicated to the study and modelling of cyclic variability in spark-ignition engines with LES, SAE paper (2011-01-1282).
[25] N. Gourdain, L. Gicquel, M. Montagnac, O. Vermorel, M. Gazaix, G. Staffelbach, M. García, J.-F. Boussuge, T. Poinsot, High performance parallel computing of flows in complex geometries – part 1: methods, Comput. Sci. Discov. 015003 (2) (2009) 26.
[26] N. Gourdain, L. Gicquel, M. Montagnac, O. Vermorel, M. Gazaix, G. Staffelbach, M. García, J.-F. Boussuge, T. Poinsot, High performance parallel computing of flows in complex geometries – part 2: applications, Comput. Sci. Discov. 015004 (2) (2009) 28.
[27] P.D. Lax, B. Wendroff, Difference schemes for hyperbolic equations with high order of accuracy, Commun. Pure Appl. Math. 17 (1964) 381–398.
[28] T. Poinsot, S. Lele, Boundary conditions for direct simulations of compressible viscous flows, J. Comput. Phys. 101 (1) (1992) 104–129.
[29] V. Granet, O. Vermorel, T. Léonard, L. Gicquel, T. Poinsot, Comparison of nonreflecting outlet boundary conditions for compressible solvers on unstructured grids, AIAA 48 (10) (2010) 2348–2364.
[30] P. Schmitt, T. Poinsot, B. Schuermans, K.P. Geigle, Large-eddy simulation and experimental study of heat transfer, nitric oxide emissions and combustion instability in a swirled turbulent high-pressure burner, J. Fluid Mech. 570 (2007) 17–46.
[31] A.W. Cook, W.H. Cabot, Hyperviscosity for shock-turbulence interactions, J. Comput. Phys. 203 (2005) 379–385.
[32] J. Smagorinsky, General circulation experiments with the primitive equations: 1. The basic experiment, Mon. Weath. Rev. 91 (1963) 99–164.
[33] S. Mendez, J. Eldredge, Acoustic modeling of perforated plates with bias flow for Large-Eddy Simulations, J. Comput. Phys. 228 (13) (2009) 4757–4772.
[34] S. Roux, G. Lartigue, T. Poinsot, U. Meier, C. Bérat, Studies of mean and unsteady flow in a swirled combustor using experiments, acoustic analysis and Large Eddy Simulations, Combust. Flame 141 (2005) 40–54.
[35] G. Staffelbach, L. Gicquel, G. Boudier, T. Poinsot, Large Eddy Simulation of self-excited azimuthal modes in annular combustors, Proc. Combust. Inst. 32 (2009) 2909–2916.
[36] M. Boileau, G. Staffelbach, B. Cuenot, T. Poinsot, C. Bérat, LES of an ignition sequence in a gas turbine engine, Combust. Flame 154 (1-2) (2008) 2–22.
[37] L. Selle, G. Lartigue, T. Poinsot, R. Koch, K.-U. Schildmacher, W. Krebs, B. Prade, P. Kaufmann, D. Veynante, Compressible Large-Eddy Simulation of turbulent combustion in complex geometry on unstructured meshes, Combust. Flame 137 (4) (2004) 489–505.
[38] G. Lacaze, B. Cuenot, T.J. Poinsot, M. Oschwald, Large Eddy Simulation of laser ignition and compressible reacting flow in a rocket-like configuration, Combust. Flame 156 (6) (2009) 116–1180.
[39] G. Lacaze, E. Richardson, T. Poinsot, Large Eddy simulation of spark ignition in a turbulent methane jet Large eddy simulation of spark ignition in a turbulent methane jet, Combust. Flame 156 (10) (2009) 1993–2009.
[40] R. Maly, M. Vogel, Initiation and propagation of flame fronts in lean CH4–air mixtures by the three modes of the ignition spark, in: 17th Symposium (International) on Combustion, The Combustion Institute, Pittsburgh, 1978, pp. 821–831.
[41] R. Teets, J. Sell, Calorimetry of ignition sparks, SAE Trans. 97 (1988) 371–383.
[42] M. Metghalchi, J.C. Keck, Laminar burning velocity of propane–air mixtures at high temperature and pressure, Combust. Flame 38 (1980) 143–154.
[43] S. Jerzembeck, N. Peters, P. Pepiot-Desjardins, H. Pitsch, Laminar burning velocity at high pressure for primary reference fuels and gazoline: experimental and numerical investigation, Combust. Flame 156 (2) (2009) 292–301.
[44] P. Sagaut, S. Deck, Large-Eddy simulation for aerodynamics: status and perspectives, Phil. Trans. R. Soc. Lond. A 367 (2009) 2849–2860.
[45] O. Colin, K. Truffin, A spark ignition model for large eddy simulation based on an FSD transport equation (ISSIM-LES), Proc. Combust. Inst. 33 (2) (2011) 3097–3104.
[46] J.E. Dec, Advanced compression–ignition engines – understanding the in-cylinder processes, Proc. Comb. Inst. 32 (2009) 2727–2742.
[47] J.L. Lumley, Stochastic Tools in Turbulence, Academic Press, New York, 1970.
[48] R.J. Blint, The relationship of the laminar flame width to flame speed, Combust. Sci. Tech. 49 (1986) 79–92.